Metrol. Meas. Syst., Vol. 31 (2024) No. 1, pp. 37–50
DOI: 10.24425/mms.2023.148540

PAN POLSKA AKADEMIA NAUK

METROLOGY AND MEASUREMENT SYSTEMS
Index 330930, ISSN 0860-8229
www.metrology.wat.edu.pl

M&MS

EFFICIENT GREEN UPCONVERSION EMISSION IN TRANSPARENT TeO_2-GeO_2 GLASS-CERAMIC OBTAINED BY BILLET EXTRUSION

Magdalena Leśniak[1)], Lesly G. Jiménez[1)], Bartłomiej Starzyk[1)], Patryk Szymczak[1)], Carlos Vázquez-López[2)], Marcin Kochanowicz[3)], Marta Kuwik[4)], Joanna Pisarska[4)], Wojciech A. Pisarski[4)], Dominik Dorosz[1)]

1) Faculty of Materials Science and Ceramics, AGH University of Science and Technology, 30 Mickiewicza Ave., 30-059 Krakow, Poland (✉ *mlesniak@agh.edu.pl*)
2) Department of Physics, Center for Research and Advanced Studies of the National Polytechnic Institute, Av. Instituto Politécnico Nacional 2508, Mexico City, Mexico
3) Faculty of Electrical Engineering, Bialystok University of Technology, 45D Wiejska Street, 15-351 Bialystok, Poland
4) Institute of Chemistry, University of Silesia, 9 Szkolna Street, 40-007 Katowice, Poland

Abstract

Transparent Yb^{3+}/Er^{3+} glass-ceramic was successfully obtained by the extrusion method. The extrusion of oxyfluoride tellurite-germanate glass co-doped with Yb^{3+} and Er^{3+} ions at 520°C resulted in the formation of $Ba_{0.75}Er_{0.25}F_{2.25}$ nanocrystals, leading to an increase in the upconversion (UC) emission intensity of 35 times in glass-ceramic with respect to the glass. The glass to glass-ceramic transition was confirmed by X-ray diffraction (XRD) and Transmission electron microscope (TEM). Also, the structural changes that occurred during crystallization were assessed using Fourier-transform infrared (FTIR) spectroscopy. Furthermore, the pump power and temperature UC emission dependence of glass and glass-ceramic under 976 nm laser excitation were investigated in detail. The assessments showed that i) two-phonons are involved in the UC process and ii) the temperature has a significant influence over it. The Yb^{3+}/Er^{3+} codoped glass-ceramic shows relatively high S_a and S_r values in a wide temperature range from 300 to 573 K, presenting the maximal S_a value of 3.50×10^{-3} at 573 K and the maximal S_r value of 6.30×10^{-3} at 364 K. These results suggest that the glass-ceramic is a good candidate for optical applications such as luminescent thermometry.

Keywords: glass-ceramics, extrusion method, upconversion, temperature sensor, structure-property relationship.

1. Introduction

Rare earth (RE) ions co-doped *upconversion* (UC) materials have the ability to convert infrared light into visible light, making them attractive for many applications, such as solid-state lasers [1], waveguide amplifiers [2], display devices [3], solar cells [4], biological imaging [5], biological sensing [6], detectors [7], and temperature sensors [8]. To obtain an efficient UC process, it is

Article history: received June 9, 2023; revised August 16, 2023; accepted September 26, 2023; available online February 1, 2024.

necessary to use a host matrix with low phonon energy and an optimized co-dopant concentration to avoid non-radiative transitions [9, 10]. Among the glass matrices with low phonon energy [11–14] tellurite-based glasses stand out [11, 15, 16] since they have a broad transmission region (up to around 6 μm) and the lowest phonon energy among oxide glass formers (~750 cm^{-1}) [11]. However, their low thermal stability limits their use. For that reason, the use of other dopants such as GeO_2 that increase its thermal stability and maintain its high RE solubility results very attractive [16–32]. Also, it was observed that its presence diminishes the phonon density of the glass, causing a slight enhancement in the UC emission intensity [12–15]. However, such an increase is enhanced when the glass is transformed into *glass-ceramic* (GC) since the unique ordered-disordered combination improves its optical, thermal, and mechanical properties [32, 33]. This is because of the local arrangement around the rare earth ions changes [10, 33–36]. The development of transparent glass-ceramics is essential for many applications. Among the techniques to fabricate glass-ceramics, the melting quenching of the glass followed by a thermal treatment stands out. In this method, nanocrystals grow in situ in the glass host, due to heating above the glass transition temperature [16]. Another typical method is direct doping, which consists of adding the nanocrystals to the melted glass at a quenching temperature. However, the nanocrystals should be thermally stable to succeed [17–20]. An alternative technique is the use of laser-induced crystallization, which has received great attention since allows the accurate design and control of lass crystallization [21]. For the past few decades, global efforts have focused on the development of glass-ceramic optical fiber optics co-doped with rare-earth ions. However, the manufacture of GC optical fibers with tailoring photonic properties is still a challenge [22–24]. Taking these premises into consideration, in this work a transparent glass-ceramic was fabricated using the billet extrusion method i.e., obtaining a transparent glass-ceramic with $Ba_{0.75}Er_{0.25}F_{2.25}$ nanocrystal dispersed in an oxyfluoride tellurite-germanate glass. To the best of our knowledge, this is the first time that such a technique has been employed for such a purpose. The sample was inspected with different techniques to confirm the presence of the crystalline phases and evaluate their luminescence properties. Also, we explore the possibility of using glass and glass-ceramic in thermometry applications.

2. Materials and methods

A glass billet with the molar composition of $30TeO_2$–$25GeO_2$–$10Ga_2O_3$–10ZnO–$18.8BaF_2$-$5Na_2O$–$0.4YbF_3$–$0.8ErF_3$ (in mol%) was obtained by the melt-quenching method. The glass samples were obtained for various concentrations of the ErF_3 (activator, 0.2, 0.4, 0.6, 0.8, 1.0, 1.2, 1.4 mol%), with a constant content of $0.4YbF_3$ (sensitizer). Having measured the luminescence spectra of co-doped glass samples, it was found that the sample with $0.4YbF_3$ and $0.8ErF_3$ (in mol%) revealed the most effective up-conversion. Therefore, this concentration of co-dopants was chosen for the experiment.

Ten grams of precursors, with purity over 99.99% from Sigma-Aldrich, were well mixed in a mortar and placed in a platinum crucible. After that, the crucible with the set has been heated from room temperature to 1050°C for 1h 30 min. The crucible was not been covered during melting. When the melting was completed, the liquid was quenched on a pre-heated rod mold with a diameter of 10 mm and a length of 60 mm. Then the billet was annealed at 390°C for 6 h. Finally, the sample was cooled at 10°C/h until room temperature. The glass billet was used as an extrusion preform to obtain a glass-ceramic sample. Prior to extrusion, the cylindrical billet and its surface were polished.

The glass billet was extruded in an extruder fabricated by the Czylok company. Graphite was been used as a die material for tellurite-germanate glass-ceramic extrusion. The sample was been extruded at a viscosity of about 10^8 Pa·s, below the onset of glass crystallization temperature (T_{x1}). We performed many experiments on various extruded parameters, and finally, the temperature of the heating furnace used in the extrusion was determined at 520°C. The billets were extruded into cylindrical glass-ceramic of 1 mm in diameter under a pressure of 170 kg and at a speed of 0.5 mm/min. The extruded glass-ceramic was then moved to anneal slowly at a temperature slightly below T_g to room temperature.

The *differential scanning calorimetry* (DSC) curve of the glass was obtained at 10°C/min from room temperature to 1000°C using a SETARAM Labsys thermal analyzer. The X-ray diffraction patterns of glass and glass-ceramics were measured using an X'Pert Pro X-ray diffractometer supplied by PANalytical with Cu Kα1 radiation (λ = 1.54056 Å). The X-ray tube was operated at 40 kV and 40 mA and equipped with a scintillation detector. Qualitative identification of the phase composition in the glass-ceramic and ceramic samples was performed with reference to concerning the ICDD PDF-2 database. The transmission electron micrographs were obtained using spherical aberration-corrected scanning transmission electron microscopy (ARM200F, JEOL). The infrared spectra of all samples were measured with a Bruker Optics-Vertex70 V Fourier spectrometer using the KBr pellet technique. All spectra were recorded at 128 scans with a resolution of 4 cm^{-1}. The FTIR spectra were deconvoluted using the Fityk software (0.9.8, open-source (GPL2+)). The upconverted emission spectra were recorded at room temperature using an Apollo Instrument 3 W laser diode of 975 nm. The density power of the laser was fixed at 450 mW. The laser-power dependence and read-out capability were obtained using a Stellarnet Green-Wave monochromator with λ_{exc} = 976 nm excitation. The temperature-dependent luminescence measurements were performed on an electric heater at a 300 K–573 K temperature range. The material was placed over the stainless-steel plate of the heater, and then heated with remaining there for 5 min to guarantee temperature stability. After that, the sample was irradiated at 980 nm (P_{max} = 375 mW) with a CW fiber laser (Changchun New Industries Optoelectronics Tech. Co., Ltd., Changchun, China) for obtaining luminescence spectra.

3. Results and discussion

3.1. Thermal characterization – the DSC curve of the glass

The differential scanning calorimetry curve of the oxyfluoride tellurite-germanate glass co-doped with $0.4YbF_3/0.8ErF_3$ is presented in Fig. S1. The DSC curve shows that the glass transition (Tg) occurs at 413°C. The exothermic peaks, located at 570 (Tc1) and 638°C (Tc2) are attributed to the temperature of the glass crystallization.

3.2. Structure characterization

3.2.1. X-ray diffraction

The X-ray diffraction patterns of the glass, glass-ceramic, and ceramic are presented in Fig. 1. The XRD pattern of the glass (Fig. 1a) confirms the amorphous nature of the sample since the diffraction pattern exhibits two broad bands centered at 27.8 and 48.8° of 2θ, which are typical of a glassy structure [25]. The diffraction pattern of the extruded transparent glass-ceramic sample exhibits some diffraction peaks at 25.6, 29.5, 42.3, and 50.0° of 2θ (Fig. 1b), which well match the cubic $Ba_{0.75}Er_{0.25}F_{2.25}$ crystals, presented as a circle (JCPDS no. 152-8531). However, such

diffraction peaks overlap the broad signals from the amorphous component indicating that the crystals in this sample coexist with a significant amount of an amorphous phase coming from the glass matrix. Such amorphous contribution reduces when the sample is heated over 560°C for 30 minutes (Fig. 1c), favoring the growth of $Ba_{0.75}Er_{0.25}F_{2.25}$, BaF_2 (presented as a star, JCPDS no. 720-3818), and $BaGa_2Ge_2O_8$ (presented as a triangle, JCPDS no. 009-4175) crystals phases.

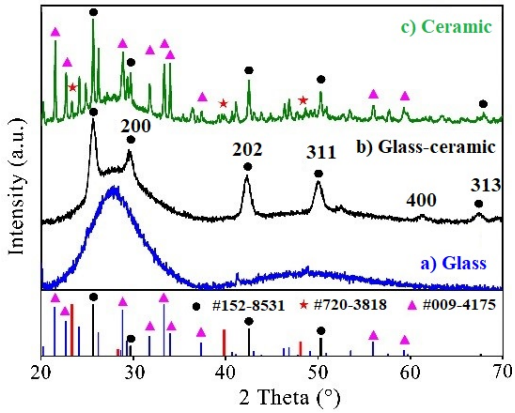

Fig. 1. X-ray diffraction patterns for Yb^{3+}/Er^{3+} co-doped a) glass, b) extruded glass-ceramic, and c) glass heated at 560°C for 30 minutes.

3.2.2. Transmission electron microscopy

Figure 2 shows TEM images of the glass-ceramic, as well as the corresponding electron diffraction patterns, and high-resolution (HRTEM) micrographs. The TEM image of the GC (Fig. 2a) confirms the presence of nanocrystals, which have a size distribution of 11.7 ±0.8 nm (Fig. S2). In the HRTEM images (Fig. 2b), the lattice fringes of (202) and (311) planes in $Ba_{0.75}Er_{0.25}F_{2.25}$ are indicated. Moreover, it is possible to distinguish an amorphous region on the sample. From the electron diffraction pattern, it is possible to confirm the presence of a crystalline phase, thus it is possible to observe the formation of faint diffraction rings (inset in Figure 2b) which will match the $Ba_{0.75}Er_{0.25}F_{2.25}$ phase. However, these are quite diffuse because of the presence of the amorphous phase [26]. All of these results are in agreement with the XRD diffraction pattern of extruded glass-ceramic co-doped with Yb^{3+}/Er^{3+} (Figure 1b).

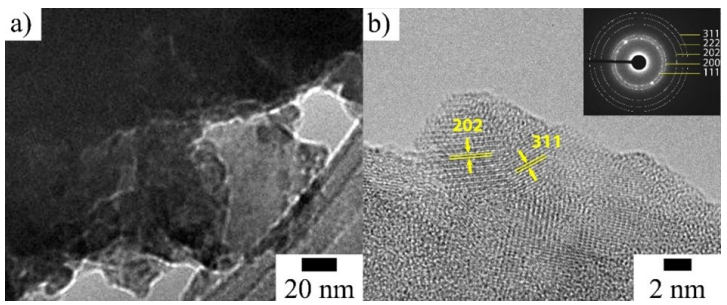

Fig. 2. TEM a) and b) HRTEM images for the extruded GC sample. The inset in b) presents five diffraction rings originating from the diffraction of the lattice face with the Miller indices of (311) (222) (202) (200), and (111) – inset in 2b.

3.2.3. FTIR spectra

The infrared deconvoluted spectra of glass and glass-ceramic are shown in Figure 3. The FTIR spectra between 400 and 1100 cm^{-1} have mainly two bands centered around 500 and 770 cm^{-1}. These bands correspond to the vibrational modes of tellurite, germanate, and gallate structural units [27–29], and their deconvoluted components are presented in Table S1 [27–30]. The deconvolution of the spectra exhibits slight changes in the vibrations ascribed to symmetric and asymmetric stretching vibrations of Ge–O–Ge, located in the 400 – 600 cm^{-1} range [27]. While the scattering bands at 642, 682, and 748 cm^{-1}, which correspond to six-coordinated Ge atoms, the TeO_4 trigonal bipyramid structure – [TeO_4]tbps, and δ(Te–O^-) of the TeO_3 trigonal pyramid structure – [TeO_3]tps respectively, increases in the glass-ceramic and ceramic samples (Figs. 3b and S3). The most evident increment occurred at 745 cm^{-1} suggesting that[TeO_3]tps units grew, triggering changes in the RE^{3+} ions arrangement that could influence the optical properties [28, 29]. On the other hand, the band between 750 and 950 cm^{-1} decreases and shifts to higher wavenumbers, which could be associated with the reduction of the bridging Ge–O–Ge of GeO_4 tetrahedra in glass-ceramic and ceramic samples, because the thermal treatment favors other vibrations (Fig. S3) [30]. These results confirm that the temperature required to extrude the transparent glass ceramic causes changes in the structural components that could impact the upconverted emission.

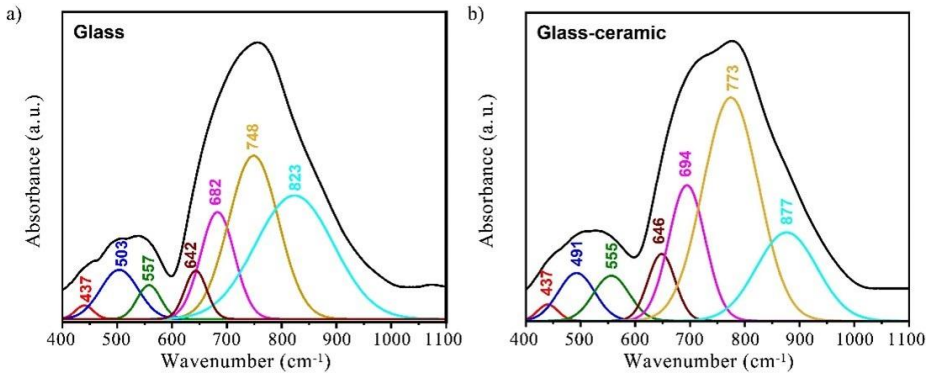

Fig. 3. FTIR spectra of Er^{3+}/Yb^{3+} co-doped a) glass, b) extruded glass-ceramic.

3.3. Optical characterization

3.3.1. Upconversion luminescence

The *upconversion* (UC) spectra of the glass, transparent glass-ceramic, and ceramic based on oxyfluoride tellurite-germanate glass co-doped with 0.4Yb^{3+}/0.8Er^{3+} under 976 nm excitation are presented in Fig. 4. All UC spectra exhibit the typical upconverted emission of erbium at 525 nm ($^2H_{11/2} \rightarrow 4I_{15/2}$), 548 nm ($^4S_{3/2} \rightarrow {}^4I_{15/2}$), and 668 nm ($^4F_{9/2} \rightarrow {}^4I_{15/2}$). The luminescence intensities of green and red emissions are higher in glass-ceramic compared to glass and ceramic. In addition, the Stark splitting observed in the glass-ceramic confirms the ordered local field environment of rare-earth ions, which reduces the probability of the multiphonon nonradiative relaxation of erbium and ytterbium ions [31]. The enhancement of the upconversion luminescence of the glass-ceramic compared to the glass may be correlated with the partial incorporation of erbium ions in the low phonon energy nanocrystals of the $Ba_{0.75}Er_{0.25}F_{2.25}$ [32]. Generally, an

increase in heat treatment temperature of the glass leads to the crystallization of more than one kind of crystal, as we observed in XRD of $Ba_{0.75}Er_{0.25}F_{2.25}$, BaF_2, and $BaGa_2Ge_2O_8$ (Fig. 1c) and confirmed by FTIR. However, this causes the presence of more defects in the crystals' surface potentiating other non-radiative vibrations and resulting in a quenching effect [32].

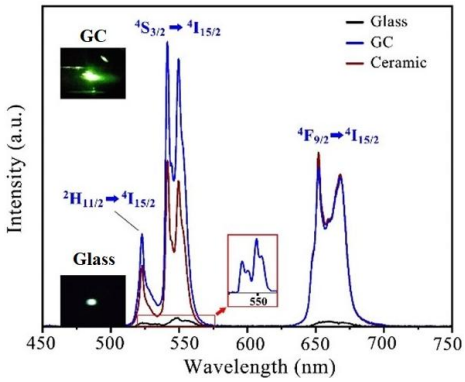

Fig. 4. Upconversion spectra of Yb^{3+}/Er^{3+} co-doped a) glass, b) extruded glass-ceramic, and c) glass heated at 560°C under 967 nm at room temperature.

3.3.2. Excitation mechanism of UC

To better understand the upconversion mechanism, the dependence of the emission intensities on the pump power under 980 nm laser excitation was measured in the co-doped with Yb^{3+}/Er^{3+} glass and extruded glass-ceramic. The relation between UC intensity (I) and pump power (P) allows the use of the $I \sim P^n$ formula, where n is the number of pumping photons required to populate the upper emitting energy levels [33]. Such dependence on glass and extruded glass-ceramic is presented in Fig. 5. The slope of the green (525 nm, 548 nm, presented as a square and a circle, respectively) and red (668 nm, presented as a triangle) emissions for glass is 1.9, 1.6, and 1.5, respectively (Fig. 5a), and the slopes of the glass-ceramic are 1.5 (525 nm, square), 1.4 (548 nm, circle), and 1.52 (668 nm, triangle) in Fig. 5b. This indicates that in both cases, two two-photons are involved in the upconversion process.

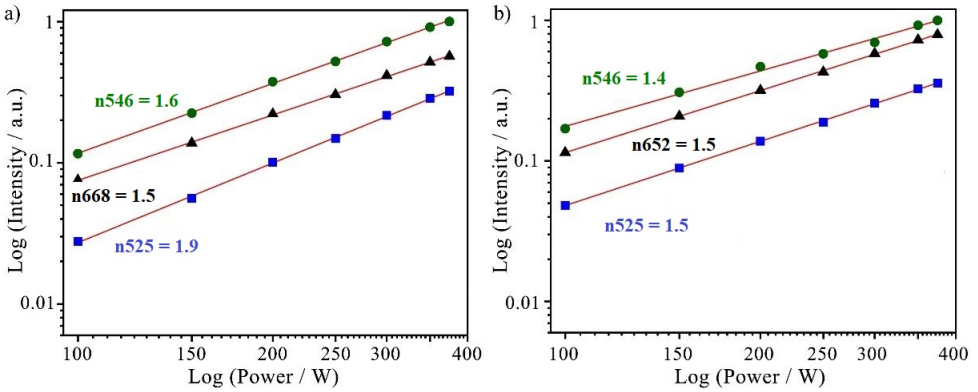

Fig. 5. Dependence of emission intensity on pump power for glass and extruded glass-ceramic.

To give a profound insight into the upconversion mechanism, the energy level diagram of the Er^{3+}–Yb^{3+} system is displayed in Fig. 6. First, Yb^{3+} absorbs one photon and it is excited from the $^2F_{7/2}$ to $^2F_{5/2}$state. This process is called *ground-state absorption* (GSA) and involves only one ion. Green emission is associated with upconversion processes, which occur according to the following processes: the $^4I_{11/2}$ level is populated by GSA: $^4I_{15/2}(Er^{3+})$+ photon $\rightarrow{}^4I_{11/2}(Er^{3+})$ and energy transfer (ET): $^2F_{5/2}(Yb^{3+})$+$^4I_{15/2}(Er^{3+})$ $\rightarrow$ $^2F_{7/2}(Yb^{3+})$+$^4I_{11/2}(Er^{3+})$. The population of the $^4F_{7/2}(Er^{3+})$ level is followed by energy transfer upconversion (ETU): $^4I_{11/2}(Er^{3+})$+$^4I_{11/2}(Er^{3+})$ $\rightarrow{}^4I_{15/2}(Er^{3+})$+$^4F_{7/2}(Er^{3+})$, excited state absorption (ESA): $^4I_{11/2}(Er^{3+})$+ photon $\rightarrow{}^4F_{7/2}(Er^{3+})$ and energy transfer: $^2F_{5/2}(Yb^{3+})$+$^4I_{11/2}(Er^{3+})$ $\rightarrow{}^2F_{7/2}(Yb^{3+})$+$^4F_{7/2}(Er^{3+})$. Subsequently, both non-radiative relaxations $^4F_{7/2}$ $\rightarrow$ $^2H_{11/2}$, and $^4S_{3/2}$ give emissions in the range of 525 nm ($^2H_{11/2}$ $\rightarrow{}^4I_{15/2}$), 548 nm ($^4S_{3/2}$ $\rightarrow{}^4I_{15/2}$), and 668 nm ($^4F_{9/2}$ $\rightarrow{}^4I_{15/2}$) [32].

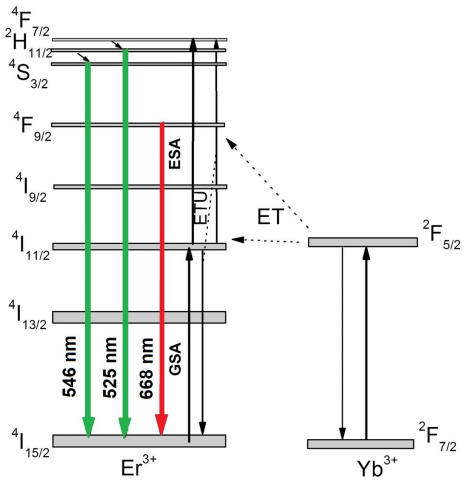

Fig. 6. Energy level diagrams with the mechanism of energy transfer for Yb^{3+}/Er^{3+} co-doped glass pumped at 976 nm.

3.3.3. Optical thermometry

Optical thermometry in terms of the *fluorescence intensity ratio* (FIR) method is suitable for erbium ions [32]. It benefits from the two *thermally coupled energy levels* (TCELs) of erbium ions: $^2H_{11/2}$, and $^4S_{3/2}$. The relationship between the FIR value of the two green-emitting bands in the upconversion spectrum of Er^{3+} and temperature is given in (1) [33].

$$\mathrm{FIR} = B \exp\left(-\frac{\Delta E}{k_B T}\right) \tag{1}$$

where FIR is the value of the ratio of the $^2H_{11/2}$ $\rightarrow$ $^4I_{15/2}$, and $^4S_{3/2}$ $\rightarrow{}^4I_{15/2}$ transitions, B is a constant, ΔE represents the energy gap between $^2H_{11/2}$ and $^4S_{3/2}$, k_B is the Boltzmann constant, and T is the absolute temperature [33].

Following this approach, the upconversion spectra of glass and extruded glass-ceramic under 976 nm excitation were measured from 300 K to 573 K for their application as optical temperature sensors (Figs. 7a,b). The FIR ratios in the function of the temperature for glass and glass-ceramic were presented in Fig. 8a. It can be seen that the intensity of green and red emissions decreases

with an increase in temperature for both samples *i.e.*, glass and glass-ceramic. The temperature-dependent green and red luminescence quenching may be connected with nonradiative relaxation processes at higher temperatures [34, 35].

In addition, the fitting lines are well matched with the experimental data, and the energy gap ΔE between the two TCELs of the $^2H_{11/2}$ and $^4S_{3/2}$ are estimated to be 672 cm^{-1} and 663.6 cm^{-1} for glass and glass-ceramic, respectively.

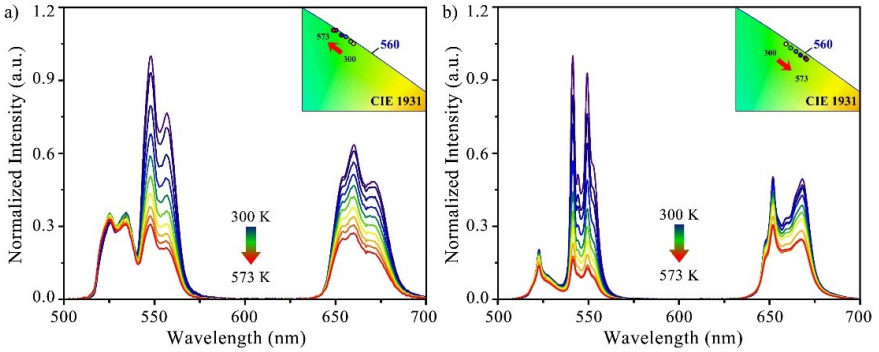

Fig. 7. Temperature-dependent upconversion emission spectra for a) glass and b) extruded glass-ceramic in the wavelength range of 500-700 nm.

The relationship between the change in FIR value with temperature for glass and glass-ceramic (Figs. 8a and b, respectively) could also be quantitatively evaluated with sensitivity S. The absolute sensitivity S_a and relative sensitivity S_r can be defined according to (2), and (3), respectively [36]:

$$S_a = \left|\frac{\mathrm{d\,FIR}}{\mathrm{d}T}\right| = \mathrm{FIR}\frac{\Delta T}{k_B T^2}, \tag{2}$$

$$S_r = \left|\frac{1}{\mathrm{FIR}}\right|\left|\frac{\mathrm{d\,FIR}}{\mathrm{d}T}\right| = \frac{\Delta E}{k_B T^2}. \tag{3}$$

S_a and S_r of glass and glass-ceramic were obtained according to the definition of sensitivity and are shown in Figures 8c, and 8d, respectively. The Yb^{3+}/Er^{3+} co-doped glass shows relatively high S_a and S_r values in a wide temperature range from 300 to 600 K, presenting the maximal S_a value of 4.58×10^{-3} at 477 K and the maximal S_r value of 10.60×10^{-3} at 300 K compared to the glass-ceramic sample, presenting the maximal S_a value of 3.50×10^{-3} at 573 K and the maximal S_r value of 6.30×10^{-3} at 364 K (Tables 1, 2). However, it should be mentioned that despite the sensitivity of the glass-ceramic being lower than glass, the emission intensity of GC is 35 times higher.

In particular, as a comparison, several typical Yb^{3+}/Er^{3+} systems for optical thermometry-based TCELs are listed in Tables 1 and 2. The calculated maximum sensitivity for glass in this temperature is significantly higher with respect to the TeO_2–ZnO–Nb_2O_5–Er_2O_3–Yb_2O_3 [37], TeO_2–GeO_2–K_2O–$10Bi_2O_3$–Er_2O_3–Yb_2O_3 [38], TeO_2–LaF_3–NaF–TiO_2–Er_2O_3–Yb_2O_3 [39], and PbO–GeO_2–Ga_2O_3–Er_2O_3–Yb_2O_3 [40] glass systems. The optical thermometry parameters of some glass-ceramics and nanophosphors are presented in Table 2. As can be seen, they exhibit lower values at a given temperature than extruded tellurite-germanate glass-ceramic. That means that the glass and extruded glass-ceramic could be in favour of application in measuring temperature with very high sensitivity.

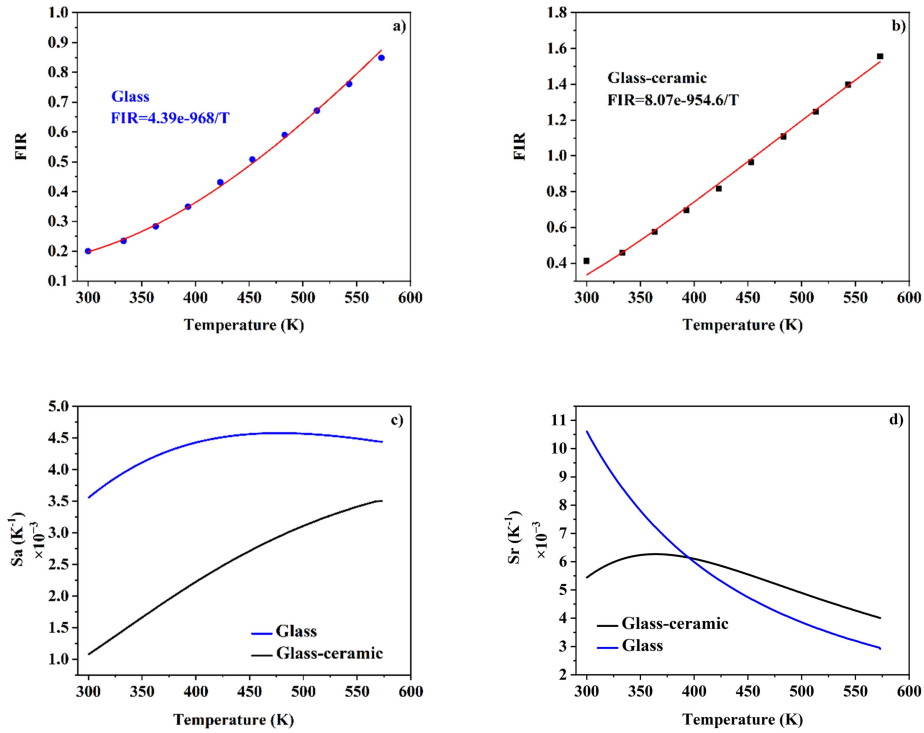

Fig. 8. a), b) Plot of FIR value versus absolute temperature and fitting curves, as well as c), d) relative temperature sensitivity Sa and Sr of glass and extruded glass-ceramic at various temperatures.

Table 1. Maximum sensitivity values for different Yb^{3+}/Er^{3+} co-doped glasses based on FIR.

Glass	Maximum Sensitivity (10^{-3} K^{-1})	Temperature (K)	References
Tellurite-germanate	10.60	300	This work
TeO_2–ZnO–Nb_2O_5–Er_2O_3–Yb_2O_3	9.50	363	[37]
TeO_2–GeO_2–K_2O–10Bi_2O_3–Er_2O_3–Yb_2O_3	8.90	473	[38]
TeO_2–LaF_3–NaF–TiO_2–Er_2O_3–Yb_2O_3	8.72	558	[39]
PbO–GeO_2–Ga_2O_3–Er_2O_3–Yb_2O_3	7.00	550	[40]

Table 2. Maximum sensitivity values for different Yb^{3+}/Er^{3+} co-doped glass-ceramic and phosphor materials based on FIR.

Glass-Ceramic	Maximum Sensitivity (10^{-3} K^{-1})	Temperature (K)	References
Tellurite-germanate	6.30	364	This work
SiO_2–Al_2O_3–AlF_3–Na_2CO_3–NaF–Gd_2O_3–Er_2O_3-Tm_2O_3	1.00	334	[41]
$NaScF_4$: Yb/Er	3.30	298	[42]
Y_2O_3: Er	2.70	298	[43]
$NaBiF_4$: Yb/Er/Fe	5.30	303	[44]

4. Conclusions

A transparent glass-ceramic co-doped with Yb^{3+}/Er^{3+} ions was successfully obtained by the billet extrusion method. The nanocrystals are well mixed in the oxyfluoride TeO_2–GeO_2 glass matrix. These have a size of ~11 nm and fit well with $Ba_{0.75}Er_{0.25}F_{2.25}$ crystals. Also, the FTIR confirms changes in the structural arrangement. Such changes influence the cooperative energy transfer between Yb^{3+} and Er^{3+} in the transparent glass-ceramic leading to an enhancement in the upconverted emission spectra. The results show a promising use in different optical applications. One of them is the optical thermometry as we observed, since the sensitivity of this material is 6.30×10^{-3} 364 K.

Funding

The research activity was granted by the National Science Centre, Poland No. 2020/39/D/ST5/02287, as well as in part by the "Excellence Initiative – Research University" for the AGH University of Science and Technology grant no. 501.696.7996 D2 L34 ID4844.

Acknowledgements

The authors acknowledge the technical assistance of Dr. Daniel Bahena from Laboratorio Avanzado de Nanoscopía Electrónica (LANE) and Ana Bertha Soto from the Department of Physics, both from the Center for Research and Advanced Studies of the National Polytechnic Institute, Mexico City, Mexico.

References

[1] Wang, Y., Li, W., Pan, L., Yu, J., & Zhang, R. (2013). Optimization of concentration and length of laser medium in diode-end-pumped solid-state lasers considering energy-transfer-upconversion effects. *Optik (Stuttg)*, *124*, 1445–1449. https://doi.org/10.1016/j.ijleo.2012.03.071

[2] Jia, Y., Yao, Y., Wang, S., Ren, Y., Zhao, X., & Chen, F. (2021). Dual-color upconversion luminescence emission from Er:LiNbO3 on-chip ridge waveguides. *Results in Physics*, *27*, 104526. https://doi.org/10.1016/j.rinp.2021.104526

[3] Mushtaque, S. G. M., Kadam, A. R., & Dhoble, S. J. (2023). High color purity and color tunability in Sm3+/Eu3+ activated/ co-activated Sr6Ca4(PO4)6F2 phosphor for WLED and display devices application. *Journal of Molecular Structure*, *1274*, 134510. https://doi.org/10.1016/j.molstruc.2022.134510

[4] Li, S., Li, Y., Sun, X., Li, Y., Deng, F., & Tao, X. (2023). Hole transport layer-free carbon-based perovskite solar cells with high-efficiency up to 17.49% in air: From-bottom-to-top perovskite interface modification. *Chemical Engineering Journal*, *455*, 140727. https://doi.org/10.1016/j.cej.2022.140727

[5] Xu, R., Cao, H., Lin, D., Yu, B., & Qu, J. (2022). Lanthanide-doped upconversion nanoparticles for biological super-resolution fluorescence imaging. *Cell Reports Physical Science*, *3*, 100922. https://doi.org/10.1016/j.xcrp.2022.100922

[6] Yang, J., Zu, L., Li, G., Zhang, C., Ge, Z., Wang, W., Wang, X., Liu, B., Xi, N., & Liu, L. (2023). Upconversion optogenetics-driven biohybrid sensor for infrared sensing and imaging. *Acta Biomater.*, *158*, 747–758. https://doi.org/10.1016/j.actbio.2023.01.017

[7] Zhou, J., Cai, H., Ren, Y., Li, S., Jiang, C., Lv, Z., Wang, T., Qu, G., Cai, P., Tan, Y., Shi, J., Xin, M., Miao, X., & Liu, Q. (2023). Effect of micro-range transmission on the imaging sharpness of near-infrared upconversion thin-film silicon-based detectors. *Optics Communications*, *529*, 129108. https://doi.org/10.1016/j.optcom.2022.129108

[8] Zhang, Y., Guo, Y., Zheng, X., Wang, P., & Liu, H. (2023). Bright upconversion luminescence performance of $Yb^{3+}/Tm^{3+}/Gd^{3+}/Er^{3+}$ doped AWO_4 (A=Sr or Ca) phosphor for optical temperature sensor. *Physica B: Condensed Matter*, *649*, 414467. https://doi.org/10.1016/j.physb.2022.414467

[9] Klinkov, V., Aseev, V., Semencha, A., & Tsimerman, E. (2018). Temperature sensor based on upconversion luminescence of Er^{3+}-doped fluoroaluminate glasses. *Sensors and Actuators A: Physical*, *277*, 157–162. https://doi.org/10.1016/j.sna.2018.04.048

[10] Wang, Q., Wen, J., Zheng, J., Xia, Q., Wei, C., Huang, X., Mu, Z., & Wu, F. (2022). Exploration of up-conversion thermal enhancement mechanism and application on temperature sensing of $Sc_2W_3O_{12}$: Yb^{3+}, Er^{3+} materials. *Journal of Luminescence*, *252*, 119306. https://doi.org/10.1016/j.jlumin.2022.119306

[11] Tekın, H., Süsoy, G., Issa, S. A., Ene, A., ALMisned, G., Rammah, Y. S., Ali, F. T., Algethami, M., & Zakaly, H. M. (2022). Heavy metal oxide (HMO) glasses as an effective member of glass shield family: A comprehensive characterization on gamma ray shielding properties of various structures. *Journal of Materials Research and Technology*, *18*, 231–244. https://doi.org/10.1016/j.jmrt.2022.02.074

[12] Tang, J., Sun, M., Huang, Y., Gou, J., Zhang, Yu., Li, G., Li, Y., Man, Y., Yang, J. (2017). Study on optical properties and upconversion luminescence of Er^{3+}/Yb^{3+} co-doped tellurite glass for highly sensitive temperature measuring. *Optical Materials Express*, *7*, 3238–3250. https://doi.org/10.1364/OME.7.003238

[13] Chen, R., Tian, Y., Li, B., Wang, F., Jing, X., Zhang, J., & Xu, S. (2015). 2 μm fluorescence of Ho^{3+}:$^5I_7 \rightarrow {}^5I_8$ transition sensitized by Er^{3+} in tellurite germanate glasses. *Optical Materials*, *49*, 116–122. https://doi.org/10.1016/j.optmat.2015.09.003

[14] Hou, G., Zhang, C., Fu, W., Li, G., Xia, J., & Ping, Y. (2020). Broadband mid-infrared 2.0 μm and 4.1 μm emission in Ho^{3+}/Yb^{3+} co-doped tellurite-germanate glasses. *Journal of Luminescence*, *217*, 116769. https://doi.org/10.1016/j.jlumin.2019.116769

[15] Zhang, Y., Lu, C., Feng, Y., Sun, L., Ni, Y., & Xu, Z. (2011). Effects of GeO_2 on the thermal stability and optical properties of Er^{3+}/Yb^{3+}-codoped oxyfluoride tellurite glasses. *Materials Chemistry and Physics*, 126, 786–790. https://doi.org/10.1016/j.matchemphys.2010.12.043

[16] Cruz, M.E., Li, J., Gorni, G., Durán, A., Mather, G.C., Balda, R., Fernández, J., & Castro, Y. (2021). Nd^{3+}doped- SiO_2–$KLaF_4$ oxyfluoride glass-ceramics prepared by sol-gel. *Journal of Luminescence*, *235*. 118035. https://doi.org/10.1016/j.jlumin.2021.118035

[17] Nguyen, H., Tuomisto, M., Oksa, J., Salminen, T., Lastusaari, M., & Petit, L. (2017). Upconversion in low rare-earth concentrated phosphate glasses using direct $NaYF_4$:Er^{3+}, Yb^{3+} nanoparticles doping. *Scripta Materialia*, *139*, 130–133. https://doi.org/10.1016/j.scriptamat.2017.06.050

[18] Ojha, N., Laihinen, T., Salminen, T., Lastusaari, M., & Petit, L. (2018). Influence of the phosphate glass melt on the corrosion of functional particles occurring during the preparation of glass-ceramics. *Ceramics International*, *44*(10), 11807–11811. https://doi.org/10.1016/j.ceramint.2018.03.267

[19] Lahti, V., Ojha, N., Vuori, S., Lastusaari, M., & Petit, L. (2021). Preparation of glass-based composites with green upconversion and persistent luminescence using modified direct doping method. *Materials Chemistry and Physics*, *274*, 125164. https://doi.org/10.1016/j.matchemphys.2021.125164

[20] Ojha, N., Nguyen, H., Laihinen, T., Salminen, T., Lastusaari, M., & Petit, L. (2018). Decomposition of persistent luminescent microparticles in corrosive phosphate glass melt. *Corrosion Science*, *135*, 207–214. https://doi.org/10.1016/j.corsci.2018.02.050

[21] Cao, J., Lancry, M., Brisset, F., Mazerolles, L., Saint-Martin, R., & Poumellec, B. (2019). Femtosecond Laser-Induced Crystallization in Glasses: Growth Dynamics for Orientable Nanostructure and Nanocrystallization. *Crystal Growth & Design*, *19*, 2189–2205. https://doi.org/10.1021/acs.cgd.8b01802

[22] Blanc, W., Lu, Z., Robine, T., Pigeonneau, F., Molardi, C., & Tosi, D. (2022). Nanoparticles in optical fiber, issue and opportunity of light scattering [Invited]. *Optical Materials Express*, *12*(7), 2635. https://doi.org/10.1364/ome.462822

[23] Cahoon, M.A., Meehan, B., Hawkins, T.W., McMillen, C., Antonick, P., Riman, R.E., Dragic, P.D., Digonnet, M.J.F., & Ballato, J. (2022). (Invited) On the evolution of nanoparticles in nanoparticle-doped optical fibers. *Optical Materials: X*, *16*, 100202. https://doi.org/10.1016/j.omx.2022.100202

[24] Blanc, W., Gyu Choi, Y., Zhang, X., Nalin, M., Richardson, K.A., Righini, G.C., Ferrari, M., Jha, A., Massera, J., Jiang, S., Ballato, J., & Petit, L. (2023). The past, present and future of photonic glasses: A review in homage to the United Nations International Year of Glass 2022. *Progress in Materials Science*, *134*, 101084. https://doi.org/10.1016/j.pmatsci.2023.101084

[25] Leśniak, M., Mach, G., Starzyk, B., Sadowska, K., Ragiń, T., Żmojda, J., Kochanowicz, M., Kuwik, M., Miluski, P., Jiménez, G.L., Baranowska, A., Dorosz, J., Pisarski, W., Pisarska, J., Olejniczak, Z., & Dorosz, D. (2022). The Effect of Fluorides (BaF_2, MgF_2, AlF_3) on Structural and Luminescent Properties of Er^{3+}-Doped Gallo-Germanate Glass. *Materials*, *15*, 5230. https://doi.org/10.3390/ma15155230

[26] Aguilar-Frutis, M.A., Jiménez, G.L., Padilla-Rosales, I., Alarcón-Flores, G., Falcony, C., Cabañas-Moreno, J.G. (2017). Near UV excitable Eu-doped alumina nanophosphors synthesized by the microwave assisted solvothermal technique. *Materials Research Express*, *4*. 125007. https://doi.org/10.1088/2053-1591/aa9b67

[27] Koroleva, O.N., Shtenberg, M. V., & Ivanova, T.N. (2019). The structure of potassium germanate glasses as revealed by Raman and IR spectroscopy. *Journal of Non-Crystalline Solids*, 510, 143–150. https://doi.org/10.1016/j.jnoncrysol.2019.01.017

[28] Liu, Y., Lu, Z., Xu, J., & Guo, T. (2020). Studies on the influence of structure units on the state of ytterbium ions in TeO_2-based glasses. *Journal of Materials Research*, *35*, 422–429. https://doi.org/10.1557/jmr.2020.28

[29] Yan, J., Zhao, T., Shi, N., Zhan, H., Ren, J., Zhang, Y., & Yue, Y. (2022). Impact of silicon doping on the structure and crystallization of a vanadium-tellurite glass. *Journal of Non-Crystalline Solids*, *589*, 121651. https://doi.org/10.1016/j.jnoncrysol.2022.121651

[30] Işsever, U.G., Kilic, G., Peker, M., Ünaldi, T., & Aybek, A.Ş. (2019). Effect of low ratio V^{5+} doping on structural and optical properties of borotellurite semiconducting oxide glasses. *Journal of Materials Science: Materials in Electronics*, *30*, 15156–15167. https://doi.org/10.1007/s10854-019-01889-7

[31] Cruz, M.E., Fernández, J., Durán, A., Balda, R., & Castro, Y. (2023). Optically active nano-glass-ceramic coatings of Nd^{3+} doped-$80SiO_2$-$20LaF_3$ prepared by the pre-crystallized nanoparticles sol-gel route. *Journal of Non-Crystalline Solids*, 601, 122050. https://doi.org/10.1016/j.jnoncrysol.2022.122050

[32] Chen, D., Zhou, Y., Wan, Z., Huang, P., Yu, H., Lu, H., & Ji, Z. (2015). Enhanced upconversion luminescence in phase-separation-controlled crystallization glass ceramics containing Yb/Er(Tm): $NaLuF_4$ nanocrystals. *Journal of the European Ceramic Society*, *35*, 2129–2137. https://doi.org/10.1016/j.jeurceramsoc.2015.01.021

[33] Li, X., Qiu, L., Chen, Y., Zhu, Y., Yu, H., Zhong, J., Yang, T., & Mao, Q. (2021). $LiYF_4$-nanocrystal-embedded glass ceramics for upconversion: glass crystallization, optical thermometry and spectral conversion. *RSC Advances*, 11, 2066–2073. https://doi.org/10.1039/d0ra08285f

[34] Ryszczyńska, S., Trejgis, K., Marcinka, Ł., & Grzyb, T. (2021). Upconverting SrF_2:Er^{3+} Nanoparticles for Optical Temperature Sensors. *ACS Applied Nano Materials. 4*(10), 10438–10448. https://doi.org/10.1021/acsanm.1c01964

[35] Zi, Y., Yang, Z., Xu, Z., Bai, X., Ullah, A., Khan, I., Haider, A.A., Qiu, J., Song, Z., Wang, Y., & Cun, Y. (2021). A novel upconversion luminescence temperature sensing material: Negative thermal expansion Y2Mo3O12:Yb 3+, Er3+ and positive thermal expansion Y2Ti2O7:Yb 3+, Er3+ mixed phosphor. *Journal of Alloys and Compounds*, 880, 160156. https://doi.org/10.1016/j.jallcom.2021.160156

[36] Chen, S.Y.Z., Song, W.H., Cao, J.K., Hu, F.F., & Guo, H. (2020). Highly sensitive optical thermometer based on FIR technique of transparent NaY_2F_7:Tm^{3+}/Yb^{3+} glass ceramic. *Journal of Alloys and Compounds*, *825*(5), 154011. https://doi.org/10.1016/j.jallcom.2020.154011

[37] Wu, T., Tong, R., Liao, L., Huang, L., Zhao, S., & Xu, S. (2017). A Point Temperature Sensor Based on Upconversion Emission in Er^{3+}/Yb^{3+} Codoped Tellurite-Zinc-Niobium Glass. *Sensors*, *17*(6), 1253. https://doi.org/10.3390/s17061253

[38] Manzani, D., Da Silveira Petruci, J. F., Nigoghossian, K., Cardoso, A. A., & Ribeiro, S. J. L. (2017). A portable luminescent thermometer based on green up-conversion emission of Er^{3+}/Yb^{3+} co-doped tellurite glass. *Scientific Reports*, *7*, 41596. https://doi.org/10.1038/srep41596

[39] Tang, J., Sun, M., Huang, Y., Gou, J., Zhang, Y., Li, G., Li, Y., Man, Y., & Yang, Y. (2017). Study on optical properties and upconversion luminescence of Er^{3+}/Yb^{3+} co-doped tellurite glass for highly sensitive temperature measuring. *Optical Materials Express*, *7*(9), 3238–3250. https://doi.org/10.1364/OME.7.003238

[40] Pisarski, W.A., Pisarska, J., Lisiecki, R., & Ryba-Romanowski, W. (2016). Er3+/Yb3+ co-doped lead germanate glasses for up-conversion luminescence temperature sensors. *Sensors and Actuators A: Physical*, 252, 54–58. https://doi.org/10.1016/j.sna.2016.11.010

[41] Chengqi, E., Bu, Y., Meng, L., & Yan, X. (2017). Tm^{3+} Modified Optical Temperature Behavior of Transparent Er^{3+}-Doped Hexagonal $NaGdF_4$ Glass Ceramics. *Nanoscale Research Letters*, *12*(1), 402. https://doi.org/10.1186/s11671-017-2167-9

[42] Mao, Y., Xian, P., Jiang, L., Hu, S., Tang, J., & Yang, J. (2020). Temperature sensing performance based on up-conversion luminescence in hydrothermally synthesized Yb^{3+}/Er^{3+} co-doped $NaScF_4$ phosphors. *Dalton Transactions, 49*(23), 7862–7871. https://doi.org/10.1039/D0DT00809E

[43] Liu, J., Huang, W., Xia, Z., & Xu, Y. (2020). Facile synthesis of accordion-like Y2O3:Er3+ nanothermometers for ratiometric temperature sensing applications. *Journal of Luminescence*, 223, 117207. https://doi.org/10.1016/j.jlumin.2020.117207

[44] Du, P., Zhang, Q., Wang, X., Luo, L., & Li, W. (2019). Upconversion luminescence, temperature sensing and internal heating behaviors of Er3+/Yb3+/Fe3+-tridoped NaBiF4 nanoparticles. *Journal of Alloys and Compounds*, 805, 171–179. https://doi.org/10.1016/j.jallcom.2019.07.054

SUPPLEMENTARY INFORMATION
EFFICIENT GREEN UPCONVERSION EMISSION IN TRANSPARENT TEO_2–GEO_2 GLASS-CERAMIC OBTAINED BY BILLET EXTRUSION

M. Leśniak, Lesly G. Jiménez, B. Starzyk, P. Szymczak, C. Vázquez-López,
M. Kochanowicz, M. Kuwik, J. Pisarska, W. A. Pisarski, D. Dorosz

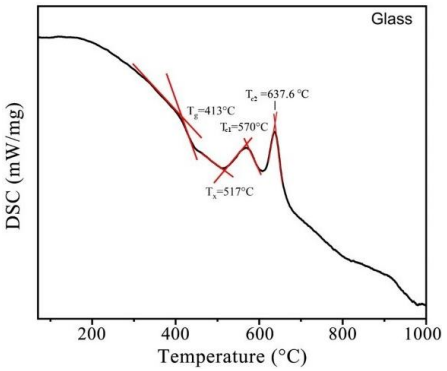

Fig. S1. DSC curve of the glass co-doped with Yb^{3+}/Er^{3+}.

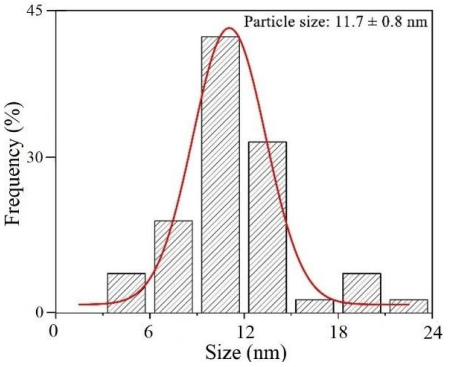

Fig. S2. The size distribution of extruded glass-ceramic doped with Yb^{3+}/Er^{3+}.

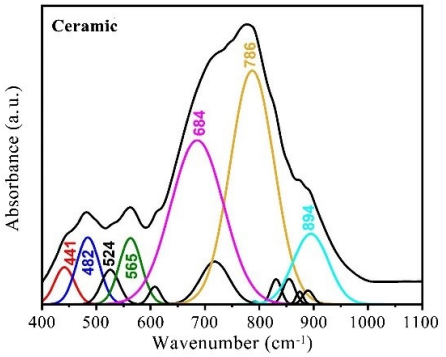

Fig. S3. FTIR spectra of Yb^{3+}/Er^{3+} co-doped germanium-tellurite matrix.

Table S1. Assignment of the bands in FTIR spectra.

Assignment	Glass	GC	Ceramic	Reference
ν_s (Ge–O–Ge)	437	437	441	[27]
ν_a (Ge–O–Ge)	557	555	565	[27]
Six-coordinated Ge atoms	642	646	—	[27]
[TeO_4] tbps	682	694	684	[28, 29]
δ(Te–O^-) of TeO_3 tps	748	773	786	[28, 30]
ν_a(Ge–O–Ge)	823	877	894	[28, 30]